Laser and Particle Beams (2017), *35*, 574–578.

doi:10.1017/S0263034617000623

Enhancement of extreme ultraviolet emission from laser irradiated targets by surface nanostructures

E. F. BARTE,[1,2] R. LOKASANI,[1,2] J. PROSKA,[1] L. MARESOVA,[1] D. KOS,[1,2] O. MAGUIRE,[2] G. JOSEPH,[2] J. SHEIL,[2] F. O'REILLY,[2] T. MCCORMACK,[2] E. SOKELL,[2] G. O'SULLIVAN,[2] J. LIMPOUCH,[1] AND P. DUNNE[2]

[1]Faculty of Nuclear Sciences and Physical Engineering, Czech Technical University in Prague, Brehova 7, 11519 Praha 1, Czech Republic
[2]UCD School of Physics, University College Dublin, Belfield, Dublin 4, Ireland

(Received 23 June 2017; Accepted 17 August 2017)

Abstract

The effects of shape and thickness of a tin surface layer and of the energy of a 170 ps neodymium:yttrium-aluminum-garnet laser pulse on the conversion efficiency (CE) into extreme ultraviolet emission in the 13.5 nm region is investigated. Whereas a CE of up to 1.16% into the 2% reflection band of multilayer Mo/Si optics was measured for a bulk Sn target at a laser energy of 25 mJ, significant CE enhancement up to 1.49% is demonstrated for a 200-nm-thick Sn layer on a microstructured porous alumina substrate.

Keywords: EUV lithography; EUV source; Microstructured Sn targets; Laser-produced plasma

1. INTRODUCTION

Laser-produced plasmas are intense sources of extreme ultraviolet (EUV) and soft X-ray emission that can be utilized for many prospective applications like surface patterning (Mocek *et al*., 2010), photoelectron spectroscopy (Dunne *et al*., 1993; Lokasani *et al*., 2015), water-window (WW) microscopy (Wachulak *et al*., 2015; Lokasani *et al*., 2016), and EUV lithography (Fomenkov *et al*., 2014; Wu & Kumar 2014). A high conversion efficiency (CE) of laser energy into the particular spectral band of interest is essential for all of the above applications. Tin plasmas have been identified as the best emitters in the 2% reflection band of multilayer Mo/Si optics at 13.5 nm (Hayden *et al*., 2006).

The presence of microstructures at the laser irradiated target surface can enhance laser absorption and influence the dynamics of the plasma plume, and thus the CE to EUV radiation can be increased and also reabsorption due to plasma opacity can be reduced. Enhancement of the soft X-ray emission from various microstructured targets irradiated by femtosecond lasers has been reported. Nishikawa *et al*., (1997) increased soft X-ray production by factors of several times by formation of a layer of porous silicon on a silicon wafer. Soft X-ray emission in the 10–20 nm range from a gold target irradiated by a 90 fs pulse of intensity 10^{16} W/cm^2 from a Ti:Sapphire laser was increased by more than ten times compared with gold foil by using a nanocylinder array structure of height 18 μm (Nishikawa *et al*., 2001). The same group used carbon nanotube targets to produce an efficient radiation source (Nishikawa *et al*., 2004a) in the WW and an alumina nanohole array to enhance radiation output in the spectral range 5–20 nm (Nishikawa *et al*., 2004b). Later Chakravarty *et al*., (2011) irradiated alumina nanohole targets by fs pulses from a Ti:Sapphire laser at intensities ranging from $\sim 3 \times 10^{16}$ to 3×10^{17} W/cm^2 to increase emission in the WW range and also of hard X rays in 2–20 keV range.

Advanced tin-containing targets have been also applied to enhance output in the 13.5 nm spectral band from plasmas produced by ns laser pulses. Nagai *et al*., (2006) demonstrated that bilayer glass/lithium (20-nm-thick)/tin (50-nm-thick) targets exhibit a sharp and strong emission in comparison with a Sn bulk target when irradiated by 10 ns neodymium: yttrium-aluminum-garnet (Nd:YAG) laser pulses of intensity 6×10^{10} W/cm^2. The same group (Okuno *et al*., 2006) reported 1.7 times higher CE at 13.5 nm into 2% bandwidth from 7% low-density SnO_2 targets (0.49 g/cm^3) irradiated by Nd:YAG laser with the same parameters as above. When a multilayer hollow nanofiber target was used and the Nd:YAG laser intensity was increased to 10^{11} W/cm^2,

Address correspondence and reprint requests to: Ellie Floyd Barte and Prof. Jiří Limpouch, Faculty of Nuclear Sciences and Physical Engineering, Czech Technical University in Prague, V Holesovickach 2, 180 00 Praha 8, Czech Republic. E-mail: elliefloydbarte@gmail.com

the CE was increased to 0.83% (Ge *et al.*, 2011). When low-density porous SnO_2 was irradiated by CO_2 laser, the narrowest bandwidth of emission at 13.5 nm was observed at an intensity of 2.9×10^{10} W/cm^2 (Ge *et al.*, 2008). Simulations showed that the presence of a porous copper nanolayer on a copper target can increase emission at WW wavelengths and at 13.5 nm when the target is irradiated by laser pulses longer than 50 ps at a laser wavelength of 532 nm and intensities up to 10^{15} W/cm^2 (Mahdieh *et al.*, 2009).

Here, we report emission properties of two different nanostructured targets coated with solid Sn layers of thicknesses 40 and 200 nm, respectively. The targets are heated by 170 ps pulses of Nd:YAG laser radiation of intensity up to 2×10^{13} W/cm^2. Significant enhancement of EUV emission in the 13.5 nm spectral band is reported for 200-nm-thick tin layers in comparison with bulk solid tin target.

2. EXPERIMENTAL DETAILS

Plasmas were produced by a *Q*-switched Nd:YAG laser ($\lambda = 1064$ nm) generating a maximum pulse energy of 240 mJ in a pulse of duration 170 ps (full width at half maximum) with a 5 Hz repetition rate. A normally incident laser beam was focused by a 10 cm anti-reflection coated BK7 convex lens. The laser spot size on the target was determined *via* the burn paper method. The laser spot has an elliptical shape with major and minor axes of lengths 130 and 80 μm, respectively. Thus, the maximum laser intensity was estimated as 2×10^{13} W/cm^2. The targets were mounted on X–Y–Z actuators, so that each laser shot was incident on a fresh target surface and any occlusion associated with laser drilling was avoided.

The emission spectra were recorded at an angle of 45° to the incident laser beam by an absolutely calibrated JENOPTIK 0.25-m flat field grazing incidence vacuum spectrometer equipped with a piezoelectric shutter and a back-illuminated charge couple device detector. This setup allowed for the determination of the absolute EUV flux within the 2% bandwidth centered on 13.5 nm. The values for in-band energy and CE are reported, assuming that the emission is isotropic into 2π steradians. The spectral range of this instrument is 9–18 nm.

The nanostructured targets were prepared by magnetron sputter deposition of a tin coating of thickness of either 40 or 200 nm onto a structured surface of a substrate. As the substrate, we used either a monolayer of closely packed polystyrene microspheres of diameter 471 nm on a silicon wafer ("microsphere target") or porous alumina with a hole diameter of 20 nm ("porous alumina target"). Target images, recorded using a scanning electron microscope (SEM) are presented in Figure 1.

3. RESULTS AND DISCUSSION

The typical measured time-integrated single-shot emission spectra from "microsphere targets" and "porous alumina targets" are presented in Figures 2 and 3. The figures demonstrate an increase in the emitted spectral energy in the 13.5 nm region as the thickness of the tin coating increases. While the emission enhancement in comparison with the tin slab is rather minor for the microsphere target (Fig. 2), the enhancement is clearly demonstrated for the 200 nm layer on the porous alumina target (Fig. 3). The strongest emission contributing in the 2% band centered on 13.5 nm has been shown to originate from transitions in Sn^{8+}–Sn^{13+} ions (Sugar *et al.*, 1992; Churilov & Ryabtsev 2006*a*,*b*). Transitions of the form $4p^6 4d^n$–$(4p^6 4d^{n-1} 4f + 4p^5 4d^{n+1})$ in these open 4*d* subshell ions overlap in adjacent ion stages, giving rise to an intense quasi-continuum feature known as an unresolved transition array (UTA) (Bauche *et al.*, 1988). This UTA is the dominant feature in the EUV spectra of Sn targets. The level of continuum is similar for all targets within the measurement accuracy.

The in-band emission energy (IEE) was calculated *via* trapezoidal integration of the emission spectra in the 2% bandwidth centered at 13.5 nm and multiplying this value

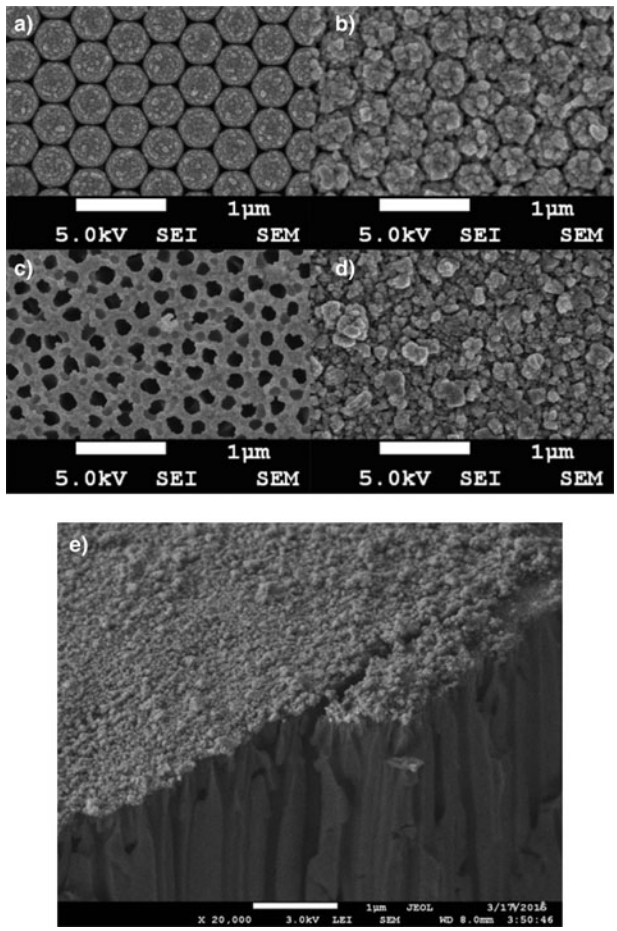

Fig. 1. SEM images of the surfaces of the nanostructured targets. Monolayer of polystyrene microspheres on silicon wafer with a tin coating of thickness 40 nm (a) and 200 nm (b). Porous alumina with Sn coating of thickness 40 nm (c) and 200 nm (d). In panel (e) a porous alumina taget with a 200 nm tin coating is displayed at a viewing angle of 45°.

https://doi.org/10.1017/S0263034617000623 Published online by Cambridge University Press

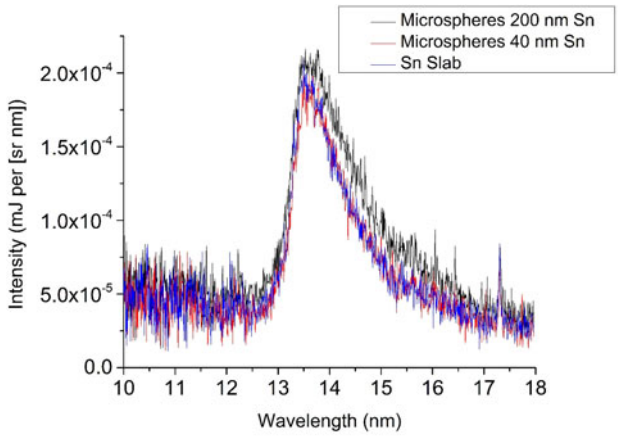

Fig. 2. Spectra emitted from "microsphere targets" (monolayer of polystyrene microspheres on silicon wafer coated by Sn layers of thickness 40 and 200 nm) and from a bulk Sn target irradiated by laser pulses of energy 26 mJ.

by 2π, assuming isotropic emission (Hayden 2007). The IEE increases with the laser energy for all targets. However, the CE reaches a maximum at relatively low laser energies 25–50 mJ. It is demonstrated in Figure 4 that the CE is increased in comparison with the bulk Sn target for all nanostructured targets with the exception of the microsphere target covered with the thin 40-nm-thick Sn layer. The thicker coating is preferred for both microstructure types, as the depth of the heated layer is thicker than 40 nm; thus, the number of Sn emitters is increased and also the decrease in density of the emitting plasma due to expansion is smaller. At the lowest laser energy, the enhancement in laser absorption is compensated by the small Sn layer thickness and the CE is approximately the same as for the bulk Sn target. However, for the 200-nm layer thickness at the lowest laser energy, the CE is increased by 21% compared with the bulk Sn target. For laser energies of 50 mJ and higher, the use of the "porous alumina target" is clearly preferential.

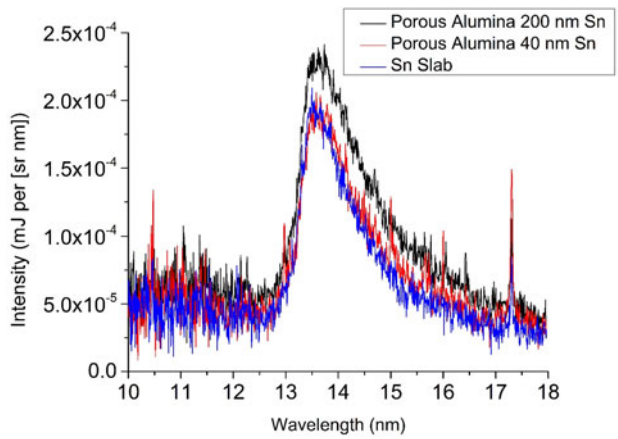

Fig. 3. Spectra emitted from "porous alumina targets" (porous alumina coated by Sn layers of thickness 40 and 200 nm) and from a bulk Sn target irradiated by laser pulses of energy 26 mJ.

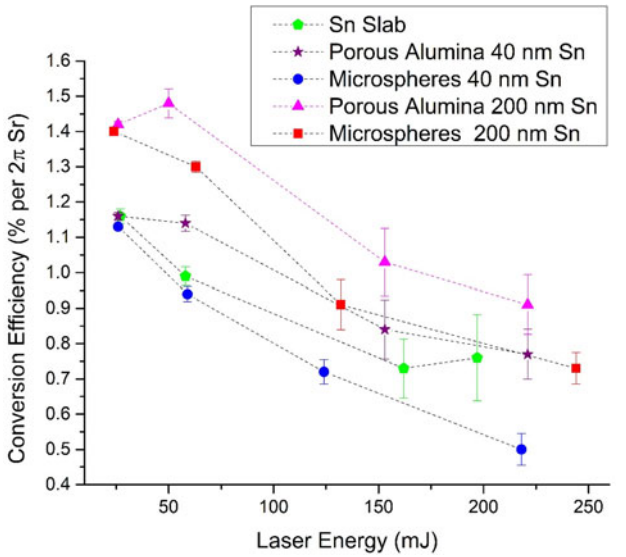

Fig. 4. In-band conversion efficiency (CE) of all nanostructured targets compared with a bulk Sn slab.

Due to its structure, tin penetrates into a certain percentage of pores up to a few tens of nm increasing the effective thickness. Moreover the heated surface Sn layer is not only expanding outwards but can be also pushed into the pores and thus the outward expansion is reduced. A clear maximum of the CE is demonstrated for a laser energy of 50 mJ with the porous alumina target covered with the 200-nm-thick Sn layer, the CE is increased to 1.49% into 2π steradians, which is 28% higher than the maximum CE obtained for the bulk Sn target. At higher laser energies, the emission from the porous alumina target is clearly the best probably due to better hydrodynamic behavior and, above 100 mJ, the CE for thinner Sn layers is roughly equal to that of microsphere targets covered by thicker Sn layers.

The measured absolutely calibrated temporally and spatially integrated emission spectra from porous alumina and microsphere targets, both covered by 200-nm-thick Sn layers, are presented in Figures 5 and 6, respectively. At the lowest laser energy of 25 mJ (intensity 2.5×10^{12} W/cm^2), the spectra contain the quasi-continuum emission from the open 4*d* subshell ions Sn^{8+}–Sn^{13+}. When the laser energy is increased, Sn ions in higher ion stages are produced and narrow lines from transitions in Sn ions up to charge state 21+ appear. The Sn lines in the spectrum were identified from the literature (D'Arcy *et al.*, 2009; Suzuki *et al.*, 2010). The observed lines include the following transitions: Sn XV ($4s^24p^54d$–$4s^24p^55p$) at 11.09 and 11.38 nm, Sn XVI ($4s^24p^44d$–$4s^24p^45p$) at 10.53 nm, Sn XIX ($4s^24p^2$–$4s^24p4d$) at 14.7 nm, Sn XXI ($3d^{10}4s^24p$–$3d^{10}4s4d$) at 16.26 nm, Sn XXII ($3d^{10}4s4p$–$3d^{10}4s4d$) at 14.59, 15.65, 16.04, and at 16.43 nm. For the microsphere target, more emission lines from highly charged Sn ions are observed and these lines are more intense than for porous alumina targets at the same laser energy. This may be due to the lower thermal

https://doi.org/10.1017/S0263034617000623 Published online by Cambridge University Press

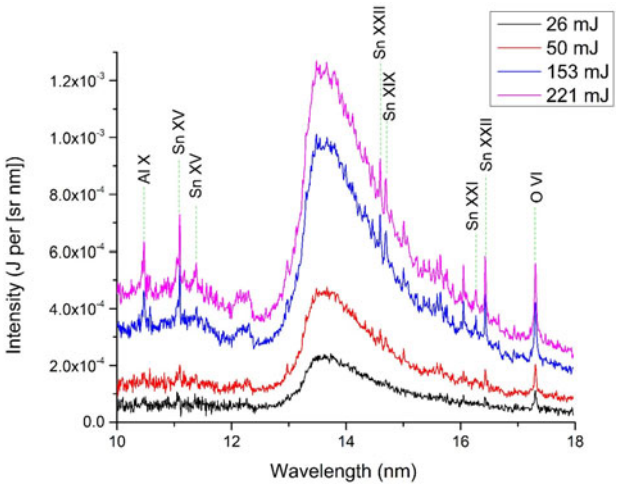

Fig. 5. Emission spectra from a porous alumina target coated with a 200-nm-thick Sn layer at various laser energies.

conductivity of the microspheres, resulting in a higher plasma temperature. For both targets at all laser energies, the spectral line of Li-like oxygen O VI at 17.3 nm due to $1s^2 2p–1s^2 3d$ transition is clearly observed. For the porous alumina target, we have identified at higher laser energies transition in Li-like Al X ($1s^2 3p–1s^2 5s$) at 10.49 nm. This line was the dominant line in our emission spectra from bulk aluminum targets.

The presented emission spectra show that for laser energies higher than 50 mJ ($I > 5 \times 10^{12}$ W/cm^2), a substantial fraction of Sn atoms is ionized to degrees higher than these that emit efficiently in-band at 13.5 nm. Though these ions may contribute to in-band emission during the recombination process after the laser pulse, both the energy spent on excessive ionization and the reduced time for which the relevant ions are present in the plasma contribute to the decrease in CE. The other factors are excessive heating and expansion of the plasma corona.

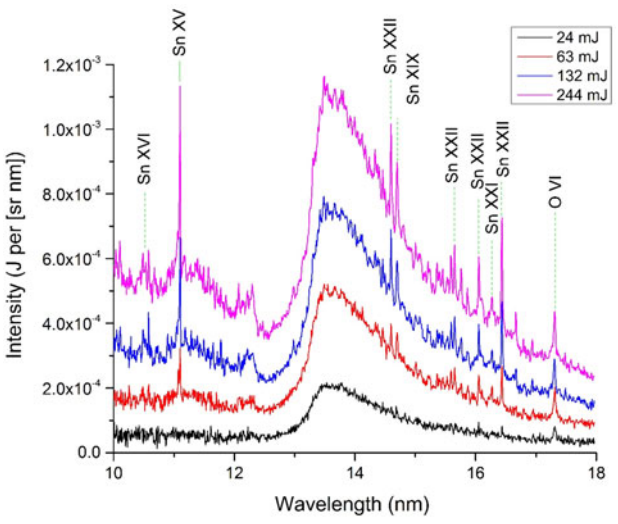

Fig. 6. Emission spectra from a polystyrene microsphere target coated with a 200 nm Sn layer at various laser energies.

4. CONCLUSIONS

We have studied the energy CE of picosecond Nd:YAG laser pulses into emission at 13.5 nm in the 2% reflection band of multilayer Mo/Si optics. We have shown that targets comprising a tin layer on a porous alumina substrate are superior to those based on a monolayer of polystyrene microspheres on a silicon wafer. We have shown that a 40-nm-thick Sn layer is too thin for efficient energy conversion to XUV emission at 13.5 nm for laser intensities higher than 2×10^{12} W/cm^2. The maximum in-band CE of 1.49%/(2π steradians), measured for 200-nm-thick Sn layer on a porous alumina substrate at a laser intensity of 4×10^{12} W/cm^2 (laser energy of 50 mJ), is 28% higher than the maximum CE measured for a bulk Sn target. For laser intensities higher than 4×10^{12} W/cm^2, the CE decreases mainly due to excessive heating and ionization of the Sn layer that is documented by the presence of lines belonging to high ionization states up to 21+ in the observed XUV spectra.

ACKNOWLEDGMENT

EFB, RL, and DK were supported by the Education, Audio-visual and Culture Executive Agency (EACEA) Erasmus Mundus Joint Doctorate Programme EXTATIC, Project No. 2012-0033. Partial support by the Ministry of Education, Youth and Sports of the Czech Republic (projects LD14032 and LG15013) is gratefully acknowledged.

REFERENCES

Bauche, J., Bauche-arnoult, C. & Klapisch, M. (1988) Unresolved transition arrays. *Phys. Scr.* **37**, 659–663.

Chakravarty, U., Arora, V., Chakera, J.A., Naik, P.A., Srivastava, H., Tiwari, P., Srivastava, A. & Gupta, P.D. (2011). X-ray enhancement in a nanohole target irradiated by intense ultrashort laser. *J. Appl. Phys.* **109**, 053301.

Churilov, S.S. & Ryabtsev, A.N. (2006*a*). Analyses of the SnIX-Sn XII spectra in the EUV region. *Phys. Scr.* **73**, 614–619.

Churilov, S.S. & Ryabtsev, A.N. (2006*b*). Analysis of the spectra of In XII-XIV and Sn XIII-XV in the far-VUV region. *Opt. Spectrosc.* **101**, 169–178.

D'Arcy, R., Ohashi, H., Suda, S., Tanuma, H., Fujioka, S., Nishimura, H., Nishihara, K., Suzuki, C., Kato, T., Koike, F., O'Connor, A. & O'Sullivan, G. (2009). Identification of 4d–5p transitions in the spectra of Sn XV–Sn XIX recorded from collisions between Sn ions and He. *J. Phys. B: At. Mol. Opt. Phys.* **42**, 165207.

Dunne, P., O'Sullivan, G. & Ivanov, V.K. (1993). Extreme-ultraviolet absorption-spectrum of Ga+. *Phys. Rev. A* **48**, 4358–4364.

Fomenkov, I.V., Brandt, D.C., Farrar, N.R., La Fontaine, B., Myers, D.W., Brown, D.J., Ershov, A. I., Bowering, N.R., Riggs, D.J., Rafac, R.J., De Dea, S., Purvis, M., Peeters, R.,

https://doi.org/10.1017/S0263034617000623 Published online by Cambridge University Press

Meiling, H., Harned, N., Smith, D., Kazinczi, R. & Pirati, A. (2014). Laser produced plasma light source development for HVM. *Proc. SPIE* **9048**, 904835.

Ge, L.Q., Bai, L.L., Fei, T., Wang, W.C., Nagai, K., Nishimura, H., Izawa, Y., Mima, K. & Norimatsu (2011). Effect of Nd:YAG laser energy on multilayer hollow nanofiber target's extreme ultraviolet conversion efficiency. *J. Macromol. Sci. B-Phys.* **50**, 1761–1770.

Ge, L.Q., Nagai, K., Gu, Z.Z., Shimada, Y., Nishimura, H., Miyanaga, N., Izawa, Y., Mima, K. & Norimatsu, T. (2008). Dry tin dioxide hollow microshells and extreme ultraviolet radiation induced by CO2 laser illumination. *Langmiur* **24**, 10402–10406.

Hayden, P. (2007). *Extreme ultraviolet source development using laser plasmas containing tin*. PhD Thesis. University College Dublin, Ireland.

Hayden, P., Cummings, A., Murphy, N., O'Sullivan, G., Sheridan, P., White, J. & Dunne, P. (2006). 13.5 nm extreme ultraviolet emission from tin based laser produced plasma sources. *Appl. Phys. Lett.* **99**, 093302.

Lokasani, R., Arai, G., Kondo, Y., Hara, H., Dinh, T. H., Ejima, T., Hatano, T., Jiang, W., Makimura, T., Li, B., Dunne, P., O'Sullivan, G., Higashiguchi, T. & Limpouch, J. (2016). Soft X-ray emission from molybdenum plasmas generated by dual laser pulses. *Appl. Phys. Lett.* **109**, 194103.

Lokasani, R., Long, E., Maguire, O., Sheridan, P., Hayden, P., O'Reilly, F., Dunne, P., Sokell, E., Endo, A., Limpouch, J. & O'Sullivan, G. (2015). XUV spectra of 2nd transition row elements: identification of 3d-4p and 3d–4f transition arrays. *J. Phys. B: At. Mol. Opt. Phys.* **48**, 245009.

Mahdieh, N.H., Fazeli, R. & Tallents, G.J. (2009). Soft x-ray enhancement from a porous nano-layer on metal targets irradiated by long laser pulses. *J. Phys. B: At. Mol. Opt. Phys.* **42**, 125602.

Mocek, T., Jakubczak, K., Kozlova, M., Polan, J., Homer, P., Hrebicek, J., Sawicka, M., Kim, I.J., Park, S.B., Kim, C.M., Lee, G.H., Kim, T.K., Nam, C.H., Chalupsky, J., Hajkova, V., Juha, L., Sobota, J., Fort, T. & Rus, B. (2010). Ablative microstructuring with plasma-based XUV lasers and efficient processing of materials by dual action of XUV/NIR-VIS ultrashort pulses. *Radiat. Eff. Defects Solids* **165**, 551–558.

Nagai, K., Gu, Q., Norimatsu, T., Fujioka, S., Nishimura, H., Miyanaga, N., Nishihara, K., Izawa, Y. & Mima, K. (2006) *Laser Part. Beams* **26**, 497–500.

Nishikawa, T., Nakano, H., Ahn, H. & Uesugi, N. (2004b). Nanohole-array size dependence of soft x-ray generation enhancement from femtosecond-laser-produced plasma. *J. Appl. Phys.* **96**, 7537–7543.

Nishikawa, T., Nakano, H., Ahn, H., Uesugi, N. & Serikawa, T. (1997). X-ray generation enhancement from a laser-produced plasma. *Appl. Phys. Lett.* **70**, 1653–1655.

Nishikawa, T., Nakano, H., Oguri, K., Uesugi, N., Nakao, M., Nishio, K. & Masuda, H. (2001). Nanocylinder-array structure greatly increases the soft X-ray intensity generated from femtosecond-laser-produced plasma. *Appl. Phys. B* **73**, 185–188.

Nishikawa, T., Suzuki, S., Watanabe, Y., Zhou, O. & Nakano, H. (2004a). Efficient water-window X-ray pulse generation from femtosecond-laser-produced plasma by using a carbon nanotube target. *Appl. Phys. B* **78**, 885–890.

Okuno, T., Fujioka, S., Nishimura, H., Tao, Y., Nagai, K., Gu, Q., Ueda, N., Ando, T., Nishihara, K., Norimatsu, T., Miyanaga, N., Izawa, Y., Mima, K., Sunahara, A., Furukawa, H. & Sasaki, A. (2006). Low-density tin targets for efficient extreme ultraviolet light emission from laser-produced plasmas. *Appl. Phys. Lett.* **88**, 161501.

Sugar, J., Kaufman, V. & Rowan, W.L. (1992). Rb-like spectra – Pd-X to Nd-XXIV. *J. Opt. Soc. Am. B* **9**, 1959–1961.

Suzuki, C., Kato, T., Sakaue, H.A., Kato, D., Sato, K., Tamura, N., Sudo, S., Yamamoto, N., Tanuma, H., Ohashi, H., D'Arcy, R. & O'Sullivan, G. (2010) Analysis of EUV spectra of Sn XIX–XXII observed in low-density plasmas in the large helical device. *J. Phys. B: At. Mol. Opt. Phys.* **43**, 074027.

Wachulak, P., Torrisi, A., Nawaz, M.F., Bartnik, A., Adjei, D., Vondrova, S., Turnová, J., Jancarek, A., Limpouch, J., Vrbova, M. & Fiedorowicz, H. (2015). A compact "water window" microscope with 60 nm spatial resolution for applications in biology and nanotechnology. *Microsc. Microanal.* **21**, 1214–1223.

Wu, B. & Kumar, A. (2014). Extreme ultraviolet lithography and three dimensional integrated circuit-A review. *Appl. Phys. Rev.* **1**, 011104.

https://doi.org/10.1017/S0263034617000623 Published online by Cambridge University Press